HAL
open science

Assessment of near Pr2/3Sr1/3MnO3 oxide in magnetic cooling

O. Chdil, M. Balli, P. de Rango, K. El Maalam, A. El Boukili, O. Mounkachi

To cite this version:

O. Chdil, M. Balli, P. de Rango, K. El Maalam, A. El Boukili, et al.. Assessment of near Pr2/3Sr1/3MnO3 oxide in magnetic cooling. International Journal of Refrigeration, 2022, 133, pp.302-312. 10.1016/j.ijrefrig.2021.10.005 . hal-03872120

HAL Id: hal-03872120

https://hal.science/hal-03872120v1

Submitted on 22 Nov 2023

HAL is a multi-disciplinary open access archive for the deposit and dissemination of scientific research documents, whether they are published or not. The documents may come from teaching and research institutions in France or abroad, or from public or private research centers.

L'archive ouverte pluridisciplinaire **HAL**, est destinée au dépôt et à la diffusion de documents scientifiques de niveau recherche, publiés ou non, émanant des établissements d'enseignement et de recherche français ou étrangers, des laboratoires publics ou privés.

Assessment of near $Pr_{2/3}Sr_{1/3}MnO_3$ oxide in magnetic cooling

O. Chdil[a,*], M. Balli[a,**], P. De Rango[b], K. El Maalam[c], A. El Boukili[d,c], O. Mounkachi[d,e]

[a]*AMEEC team, LERMA, College of Engineering and Architecture, International University of Rabat, parc Technopolis, Rocade de Rabat-Salé, 11100, Morocco.*
[b]*Université Grenoble Alpes, CNRS, Institut Néel, 38000 Grenoble, France*
[c]*Durability and Engineering of Materials center, Moroccan Foundation for Advance Science Innovation and Research (MAScIR), Rabat, Morocco*
[d]*Laboratory of Condensed Matter and Interdisciplinary Sciences (LaMCScI), Faculty of Science, Mohammed V University, Rabat, Morocco.*
[e]*MSDA, Mohammed VI Polytechnic University, Lot 660, Hay Moulay Rachid Ben Guerir, 43150, Morocco.*

Abstract

In this work, we report a detailed study of the thermodynamic performance of $Pr_{0.6}Sr_{0.4}MnO_3$ in a functional magnetic cooling system up to the theoretical limit of its magnetocaloric effect. For this purpose, a one-dimensional numerical model of the active magnetic regenerator (AMR) cycle is developed, while the required magnetocaloric properties of the oxide are calculated in the framework of mean field theory. The obtained results are deeply analyzed and then compared with the reference gadolinium metal. Particularly, it is revealed that using $Pr_{0.6}Sr_{0.4}MnO_3$ as refrigerant requires high magnetic fields to generate reasonable temperature spans for practical applications, as it was found that under a magnetic field of 8 T, the studied oxide can generate an AMR temperature span of 33 K. The thermodynamic efficiency was evaluated by directly considering the work arising from the magnetic forces between the $Pr_{0.6}Sr_{0.4}MnO_3$ regenerator and the magnetic field source, as the associated magnetic work is numerically calculated by using Altair Flux 3D software. From the obtained results, it was found that the coefficient of performance can be enhanced by a factor of two when balancing magnetic forces, despite of the moderate magnetocaloric effect shown by $Pr_{0.6}Sr_{0.4}MnO_3$ under the practical fields going from 1 to 2 T. Moreover, the hidden thermodynamic performances of this compound are also pointed out by investigating its magnetocaloric properties in the theoretical limit zone. In this way, our calculations unveil that it is possible to reach cold source temperatures under −22 °C even when using helium as heat transfer fluid.

Keywords: Magnetocaloric effect, Magnetic refrigeration, AMRR, Magnetocaloric oxides

1. Introduction

In recent years, renewable energies are evolving remarkably worldwide to tackle the global warming crisis. One of the most concerning fields is refrigeration, responsible for 20% of global electricity consumption (Dupont et al., 2019). Currently, the cooling process is based on traditional compression and expansion techniques of synthetic fluids such as chlorofluorocarbons (CFCs) and hydrochlorofluorocarbons (HCFCs) (Brück, 2005). However, the latter's are greenhouse gases, representing the main factor for raising the planet's temperature (Molina and Rowland, 1974; Seinfeld and Pandis, 2016; Velders et al., 2009). Moreover, both the Kyoto and Montreal Protocols restrict the commercialization and utilization of these hazardous refrigerants (Protocol, 1987). Furthermore, owing to their low efficiency, traditional cooling technologies require much more energy. Hence, in order to save energy and protect the environment, scientists are working on the development of more efficient clean cooling systems. In this context, magnetic refrigeration is considered as one of the best alternative solutions (Greco et al., 2019; Gschneidner Jr et al., 2005; Ismail et al., 2021; Tishin and Spichkin, 2016). This promising technology is based on utilizing the magnetocaloric effect (MCE), an intrinsic property of magnetic materials, and it can be defined as the thermal response (heating or cooling) of magnetocaloric materials when subjected to external magnetic field changes (Moya et al., 2014; Zarkevich and Zverev, 2020). Furthermore, in refrigeration and heat pumps applications, the MCE can be amplified by using the active magnetic refrigeration (AMR) cycle (Barclay, 1982; Kamran et al., 2020), on which are based the vast majority of magnetic refrigerators. The latter can be composed usually of: (i) a permanent magnet as a magnetic field source, (ii) a regenerator that contains a magnetocaloric material and heat transfer fluid channels, (iii) a hydraulic pump to ensure the fluid oscillation, and finally (iv) an electric motor to achieve the magnetization/demagnetization processes. For more details about magnetic refrigerators, we refer the interested reader to Refs. (Franco et al., 2012; Kitanovski, 2020; Kitanovski et al., 2015; Tušek and Kitanovski, 2015; Yu et al., 2010).

The thermodynamic performance of magnetic cooling devices depends strongly on the used magnetocaloric material as refrigerant. Therefore, choosing the right material based on its magnetic and magnetocaloric properties is critical for the development of this emerging cooling technique. Consequently, it is highly recommended to search for magnetocaloric materials with outstanding performance (Gottschall et al., 2019b). Specifically, advanced theoretical approaches to determine the

*Corresponding Author: O. Chdil
**Corresponding Author: M. balli
Email addresses: oumayma.chdil@uir.ac.ma (O. Chdil), mohamed.balli@uir.ac.ma (M. Balli)

Nomenclature

Roman letters

B	Magnetic field, T
C	Specific heat capacity, J kg^{-1} K^{-1}
D_h	Hydraulic diameter, m
f	Friction factor
g_J	Landé factor
h	Heat transfer coefficient, W m^{-2} K^{-1}
J	Angular momentum quantum number
k_B	Boltzmann constant, J K^{-1}
L	Length, m
M	Magnetization, μ_B f.u.$^{-1}$
m	Mass, kg
M_0	Saturation magnetization, μ_B f.u.$^{-1}$
N_c	Number of cycles
Nu	Nusselt number
p	Pressure, Pa
Pr	Prandtl number
Q_{cold}	Cooling power, W
R	Gas constant, J K^{-1} mol^{-1}
RCP	Relative cooling power, J kg^{-1}
Re	Reynolds number
S	Specific entropy, J kg^{-1} K^{-1}
t	Time, s
$\overline{T}$	Transversal average temperature, K
W	Work, J
V	Fluid velocity, m s^{-1}
x, y, z	Spatial coordinates, m

Greek letters

Δ	Finite difference
η	Efficiency
λ	Thermal conductivity, W m^{-1} K^{-1}
μ_B	Bohr magneton
ρ	density, kg m^{-3}
σ	Relative magnetization
τ	Time period, s
υ	volume, m^3
ε	Porosity of matrix

Sub- and supper-scripts

ad	Adiabatic
c	Curie
D	Debye
E	Electronic
f, r	Fluid and regenerator
FWHM	Full width half maximum
I, F	Initial and final time instants
L	Lattice
m	Magnetic
mag	Magnetization
max	Maximum
s	Solid

Abbreviations

1D	One-dimensional
AMR	Active magnetic regenerator
CCS	Clean cooling system
COP	Coefficient of performance
Gd	Gadolinium
MCE	Magnetocaloric effect
MFT	Mean-field theory
PDE	Partial differential equation

materials properties and developed models to predict the thermodynamic performance are needed before proceeding with the experimental process to minimize costs and errors. As it is already recognized, gadolinium metal (Gd) is the reference material used in the vast majority of magnetic refrigeration prototypes, and usually, any new materials are compared to its giant magnetocaloric effect near room temperature (Brown, 1976; Gottschall et al., 2019a). However, Gd and other intermetallic materials represent many issues, such as high cost, toxicity, and chemical instabilities (corrosion and oxidation) in an aqueous environment, which restrict their utilization as refrigerants in commercial applications (Balli et al., 2017; Gschneidner Jr et al., 2005; Zhang et al., 2021). Recently, the $R_{1-x}A_xMnO_3$ manganites (R = lanthanide and A = divalent alkaline earth) have attracted researchers' interest mainly due to their high chemical and mechanical stability, which compensate for their moderate magnetocaloric effect (Franco et al., 2018). This family of materials usually exhibit a relatively low adiabatic temperature change over the room-temperature range mainly because of their large specific heat combined with the second order character of their magnetic phase transition (Barman et al., 2019; Phan and Yu, 2007; Smith et al., 2012). However, their magnetocaloric properties can be significantly optimized by any electronic or structural changes caused by doping or other physical effects (Giri et al., 2019; Matte et al., 2018; Moya et al., 2013). Several research studies on manganese oxides (Balli et al., 2018; Engelbrecht et al., 2011; Legait et al., 2014; Phan et al., 2005a,b), such as $La_{2/3}(Ca,Sr)_{1/3}MnO_3$ and $Pr_{1-x}Sr_xMnO_3$, have indicated that these compounds can be utilized as active materials in magnetic refrigeration applications, as they exhibit a high transition temperature and a large magnetization (Guillou et al., 2012; Phan and Yu, 2007). Specifically, the direct implementation of these oxides (single or multilayers) as refrigerants in functional magnetic cooling devices leads to a maximum temperature span between 5 and 9.3 K under magnetic fields lower than 1.1 T (Bahl et al., 2012; Guillou et al., 2012).

It is worthy to mention that magnetic cooling has already unveiled encouraging performance at laboratory scale. Currently engineers and scientists are focusing on the development of new designs and the optimization of existing preindustrial devices (Alahmer et al., 2021; Dall'Olio et al., 2021; Huang et al., 2019; Trevizoli et al., 2017; Yu et al., 2010). In this way, the optimization of operating parameters is crucial, while numerical simula-

tions allows sensitivity analyses of the employed AMR cycles by considering several parameters such as the geometry of the regenerator matrix, characteristics of the used magnetocaloric materials, fluid's type, frequency and flow rate (Allab et al., 2005; Eustache et al., 2021; Kitanovski et al., 2014; Nielsen et al., 2011; Petersen et al., 2008; Silva et al., 2021; Tagliafico et al., 2010). Such a numerical study would enable us first to avoid the challenging experimental tests usually associated with numerous device configurations, and further to adequately simulate a material's behavior in a magnetic refrigeration device.

In this paper, the performance of $Pr_{0.6}Sr_{0.4}MnO_3$ magnetocaloric oxide in a practical magnetic refrigeration system is deeply investigated aiming to depict its real potential. This magnetocaloric oxide shows a strong chemical resistance with a curie temperature of 305 K, being suitable candidate for magnetic cooling applications near the ambient temperature. On the other hand, it exhibits an entropy and adiabatic temperature changes of about 1.6 J kg^{-1} K^{-1} and 0.8 K, respectively, in the field variation of 1 T (Daivajna and Rao, 2016; Maheswar Repaka et al., 2012). Moreover, it is worth noting also that the large electrical resistance shown by $Pr_{0.6}Sr_{0.4}MnO_3$; due to the fewer metal elements; can minimize the thermal losses caused by the eddy currents during the magnetization-demagnetization process (Guillou et al., 2012; Smith et al., 2012). This particularly motivated us to study and predict the $Pr_{0.6}Sr_{0.4}MnO_3$ thermodynamic performance in both standard and near-theoretical limit conditions, aiming to get a better understanding of its real potential in magnetic cooling. This was carried out by adopting a global approach going from predicting the needed $Pr_{0.6}Sr_{0.4}MnO_3$ properties to the determination of the thermodynamic performance. For this purpose, both an-

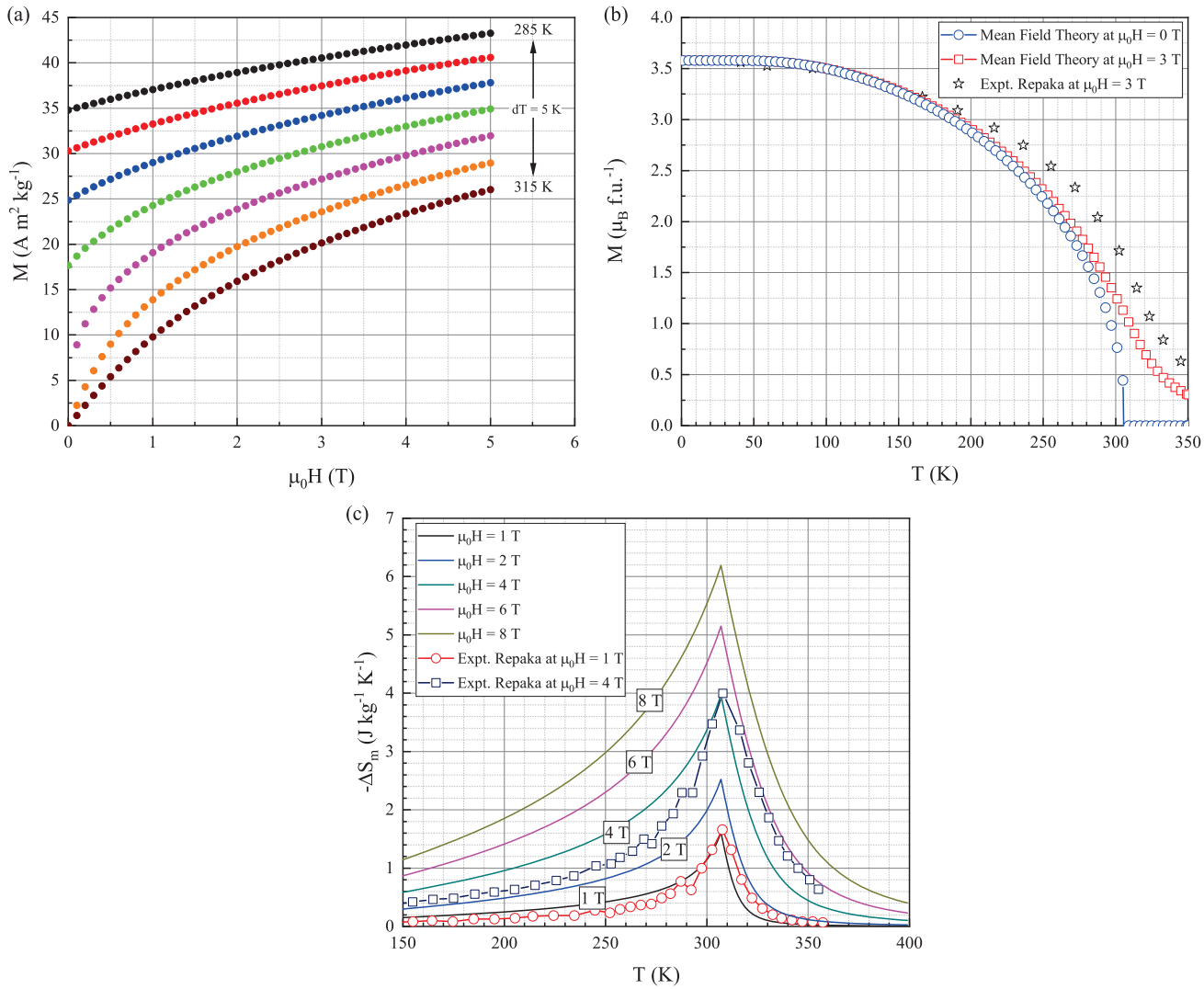

Fig. 1: (a) Magnetization as a function of temperature and applied field for $Pr_{0.6}Sr_{0.4}MnO_3$. (b) Temperature dependence of the magnetization for $Pr_{0.6}Sr_{0.4}MnO_3$ under different magnetic fields. (c) Calculated magnetic entropy changes as function of temperature under different magnetic fields. Experimental results for comparison are taken from Refs. (Maheswar Repaka et al., 2012)

alytical and numerical methods were used. This includes the mean-field theory to predict the magnetic and magnetocaloric properties, a numerical model to simulate the involved heat exchange in functional devices, and electromagnetic simulations to accurately determine the involved magnetic forces and associate works accordingly. Additionally, the calculated properties and performances are reasonably validated and compared to available experimental data. On the other hand we have also demonstrated in this paper that the $Pr_{0.6}Sr_{0.4}MnO_3$ cooling performance can be markedly enhanced (twice larger) when balancing the AMR regenerator even under relatively low magnetic fields (1T).

2. Magnetic and magnetocaloric properties of $Pr_{0.6}Sr_{0.4}MnO_3$

From a thermodynamic point of view, the full entropy S of magnetic materials is a combination of the magnetic entropy S_m, arising from the distribution of spins in the material, the lattice entropy S_L, related to the crystal lattice of the atoms, and the electronic entropy S_E, considered negligible (Waske et al., 2018). Such combination of S can be expressed as follows (Balli et al., 2012a),

$$S = S_m + S_L + S_E. \tag{1}$$

In the presence of a magnetic field, the magnetic moments are aligned, leading to the reduction of the magnetic entropy. If this process is adiabatic and reversible, then the material's full entropy is conserved, and the magnetic entropy reduction is compensated by the increase of the lattice entropy, causing an increase in the temperature of the material. The adiabatic magnetization results in a temperature variation called the adiabatic temperature change ΔT_{ad}. Besides, if the process is isothermal, the application of a magnetic field on a material without varying its temperature produces a magnetic entropy variation ΔS_m. The two parameters ΔT_{ad} and ΔS_m, and the specific heat of the material C_p as a function of both magnetic field intensity and temperature are necessary values prior to the AMR cycle simulations. In this regard, the theoretical predictions of these parameters for the here investigated oxide, employing MFT and the Neumann-Kopp's approach, are presented in the following section.

In the absence of magneto-volume effects, the magnetization of materials representing localized valence electrons can be described as a function of temperature and magnetic field, using the Brillouin function, $B_J(y)$, given by (Balli et al., 2017; De Oliveira and Von Ranke, 2010; Tishin and Spichkin, 2016),

$$\sigma = B_J(y) = \frac{2J+1}{2J}\coth\left(\frac{2J+1}{2J}y\right) - \frac{1}{2J}\coth\left(\frac{1}{2J}y\right), \tag{2}$$

with

$$y = \frac{1}{T}\left[3T_c\left(\frac{J}{J+1}\right)\sigma + \frac{g_J\mu_B J}{k_B}B\right], \tag{3}$$

where $\sigma = \dfrac{M}{M_0}$ is the relative magnetization, J is the angular momentum quantum number, T_c is the Curie temperature, g_J is the Landé factor, μ_B is the Bohr magneton, and k_B is the Boltzmann constant. The first term of Eq. (3) defines the exchange interactions, while the second term describes the Zeeman energy. The g_J parameter is generally assumed for complex magnetic substances ($g_J = 2$), while J effective value can be deduced from magnetic saturation ($3.58\,\mu_B$ f.u.$^{-1}$) (Maheswar Repaka et al., 2012), and it is supposed to be approximately 1.78. The magnetic entropy is given by Smart model (Balli et al., 2017; De Oliveira and Von Ranke, 2010; Tishin and Spichkin, 2016),

$$S_m = R \times \left[\ln\left(\frac{\sinh\left(\frac{2J+1}{2J}y\right)}{\sinh\left(\frac{y}{2J}\right)}\right) - yB_J(y)\right], \tag{4}$$

where R is the universal gas constant. Moreover, while varying the magnetic field from B_i to B_f, the corresponding change in entropy can be calculated according to the following relation,

$$\Delta S_m\left(T, \Delta B = B_f - B_i\right) = S_m\left(T, B_f\right) - S_m\left(T, B_i\right). \tag{5}$$

The resolution of the above equations allows us to represent as a function of both temperature and magnetic field, in Fig. 1(a), the magnetic isotherms, in Fig. 1(b), the thermomagnetic curves, and in Fig. 1(c), the entropy change evolution. The obtained results are compared with available experimental measurements reported mainly in Ref. (Maheswar Repaka et al., 2012). Firstly, we can observe that the studied compound exhibits a maximum entropy change ΔS_m^{max} that is peaked on its Curie temperature (T_c = 305 K) of 1.61 J kg^{-1} K^{-1} calculated using MFT in the magnetic field change of 1 T. The maximum calculated entropy change obtained from magnetization measurements of Repaka et *al.* (Maheswar Repaka et al., 2012) is about 1.648 J kg^{-1} K^{-1}, unveiling a good agreement with achieved MFT calculations. These results prove the ability of MFT-based calculations to provide a good estimation for the MCE of $Pr_{0.6}Sr_{0.4}MnO_3$ around its Curie temperature. Besides, a non-negligible difference can be observed between experimental data and MFT calculations at temperatures below T_c. Such marked deviation can be due to the MFT's simplistic nature and its inability to properly represent the magnetization at this region as several parameters are not taken into accounts, such as anisotropy effects and domain effect at 0 T (Balli et al., 2017). Furthermore, the observed peak at T_c = 305 K originates from the significant variation in magnetization near the ferromagnetism-paramagnetism (FM-PM) phase transition as shown in Fig. 1(b). Moreover, when increasing the magnetic field, the peak position remains unchanged as the phase transition taking place at T_c is second order in nature (Chmaissem et al., 2003; Martin et al., 1999; Rocco et al., 2013). In addition to the entropy change, the relative cooling power (RCP) is an important parameter that describes the efficiency of a magnetocaloric material. From Table 1, we can see the similarity

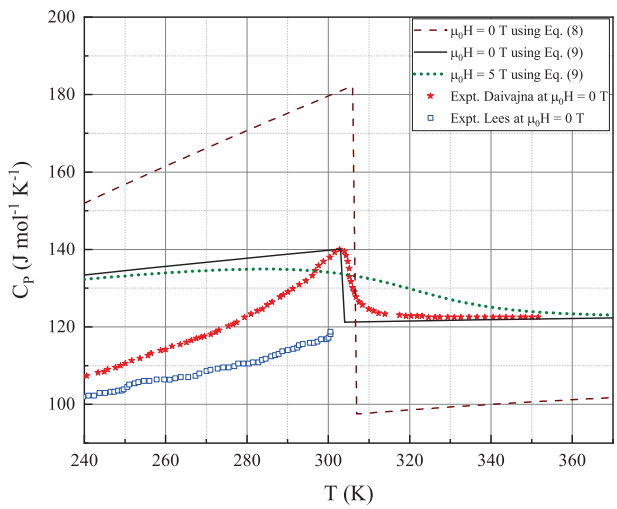

Fig. 2: Computed total specific heat capacity as function of temperature for $Pr_{0.6}Sr_{0.4}MnO_3$ in cases of: (i) absence of applied magnetic field using both Eq. (8) and Eq. (9), (ii) presence of an applied magnetic field of 5 T using Eq. (9). Results are compared with available experimental data at B = 0 T taken from Refs. (Daivajna et al., 2014; Lees et al., 1999).

of the magnetocaloric properties of $Pr_{0.6}Sr_{0.4}MnO_3$ with other manganese oxides at room temperature.

The total specific heat of a material can be described as a combination of lattice C_L, electronic C_E, and magnetic C_m contributions, as follows (Balli et al., 2017; De Oliveira and Von Ranke, 2010; Tishin and Spichkin, 2016),

$$C_P = C_m + C_L + C_E, \tag{6}$$

where the magnetic specific heat C_m is given by the following relation,

$$C_m = T\frac{\partial S_m}{\partial T}, \tag{7}$$

and using the Debye model, the lattice specific heat C_L can be expressed as,

$$C_L = 9R \times \left(\frac{T}{T_D}\right)^3 \int_0^{\frac{T_D}{T}} \frac{x^4 e^x}{(e^x - 1)^2}\, \mathrm{d}x, \tag{8}$$

where T_D is the Debye temperature. The direct use of the compound Debye temperature to calculate C_L, using Eq. (8), lead to overestimated values, as shown in Fig. 2. However, in alloys and compounds cases, we found that it is preferable to adopt Neumann and Kopp's law for a reasonable estimation of specific heat (Kopp and Graham, 1865). In this case, the lattice specific heat capacity of an A_xB_y compound can be calculated by,

$$C_{A_xB_y} = x\,C_A + y\,C_B, \tag{9}$$

where C_A and C_B are the individual lattice specific heats of constituent elements A and B, while x and y are their concentrations, respectively.

Fig. 2 shows the $Pr_{0.6}Sr_{0.4}MnO_3$ calculated specific heat versus temperature in the absence and presence of external applied magnetic fields. The reported results are compared with available experimental data taken from Refs. (Daivajna and Rao, 2016; Lees et al., 1999). The plot clearly illustrates the phase transition near the Curie point, with a decrease in its maximum value while increasing the magnetic field. The theoretical specific heat of $Pr_{0.6}Sr_{0.4}MnO_3$ at room temperature in absence of magnetic field is 140.09 J mol^{-1} K^{-1}. The latter agree nicely with the value reported by Daivajna et *al.* (Daivajna and Rao, 2016) ($\simeq$ 140 J mol^{-1} K^{-1}). However, less agreement is observed with measurement performed by Lees et *al.* (Lees et al., 1999), which could be attributed to sample imperfections. Moreover, the difference between the calculated and experimental values at temperatures below T_c is more probably associated with the challenging character of specific heat measurements. Also, this could explains the difference between the performed experimental measurements by Daivajna et *al.* (Daivajna and Rao, 2016) and by Lees et *al.* (Lees et al., 1999), reported in Fig. 2. On the other hand, it has been already reported that a structural transition occurs at low temperatures, which induces a magnetic phase transition from ferromagnetic to antiferromagnetic state resulting in a mixture of both phases (Bingham et al., 2009; Maheswar Repaka et al., 2012). However, such situation cannot be accurately described by MFT calculations (Du Trémolet de Lacheisserie et al., 2005).

The adiabatic temperature change of magnetocaloric materials that exhibit a second-order magnetic transition (i.e., continuous change in magnetization over the temperature variation) can be approached by using the following relation (Balli et al., 2017; De Oliveira and Von Ranke, 2010; Tishin and Spichkin, 2016),

$$\Delta T_{ad} = -\frac{T}{C_P}\Delta S. \tag{10}$$

Table 1: The magnetic ordering temperature and magnetocaloric parameters of $Pr_{0.6}Sr_{0.4}MnO_3$ in comparison with previous experimental reported data. Cost values are taken from Ref (Aprea et al., 2015).

Material	T_c (K)	$\mu_0 H$ (T)	$-\Delta S_{max}$ (J kg^{-1} K^{-1})	RCP (J kg^{-1})	Cost (€ kg^{-1})	Ref.
Gd	294	5	10.2	410	3000	(Dan'Kov et al., 1998)
$La_{0.8}Ba_{0.2}MnO_3$	295	5	4.45	230	-	(Ghodhbane et al., 2013)
$La_{0.5}Bi_{0.2}Sr_{0.3}MnO_3$	296	5	4.21	251	-	(Barik and Mahendiran, 2010)
$La_{0.7}Sr_{0.3}Mn_{0.93}Fe_{0.07}O_3$	296	5	4	225	-	(Barik et al., 2011)
$Pr_{0.5}Y_{0.10}Sr_{0.40}MnO_3$	310	5	3.54	247	1050	(Sakka et al., 2016)
$Pr_{0.6}Sr_{0.4}MnO_3$	294	5	4.7	261	1050	(Rocco et al., 2013)
$Pr_{0.6}Sr_{0.4}MnO_3$	305	5	4.58	269	1050	This work

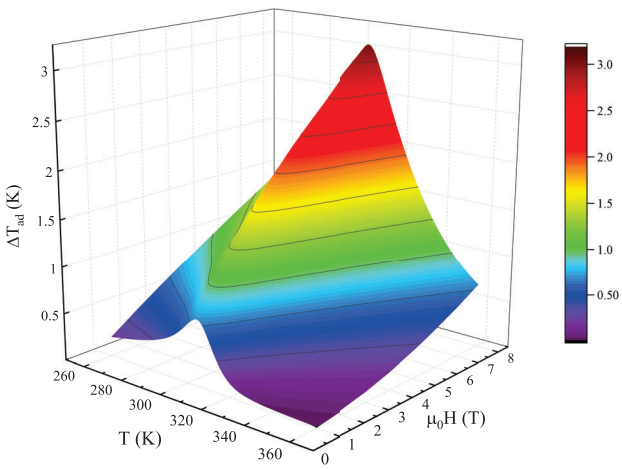

Fig. 3: Adiabatic temperature changes of $Pr_{0.6}Sr_{0.4}MnO_3$ as function of both temperature and applied magnetic field.

From Eq. (10), we can deduce that the material must exhibit a low specific heat and a high entropy change to have a giant magnetocaloric effect in term of adiabatic temperature change. In fact, a good candidate material for active magnetic refrigeration applications should possess higher ΔT_{ad}. The behavior of ΔT_{ad} as a function of the temperature and the magnetic field shown in Fig. 3, unveils the expected trends, as both a maximum around the transition temperature and an increase of ΔT_{ad} with respect to the applied magnetic field are observed.

For $Pr_{0.6}Sr_{0.4}MnO_3$, ΔT_{ad} increases while increasing the magnetic field, and exhibits a linear variation with a value of 0.8 K under 1 T and 2.64 K under 6 T at 305 K. The linear behaviour of ΔT_{ad} means that large thermal effect can be extracted under high magnetic field. The obtained experimental value of ΔT_{ad} by Daivajna et *al.* (Daivajna and Rao, 2016) is 2.2 K under an applied magnetic field of 6 T. Such achieved agreement between experimental measurements and theoretical calculations indicates the reliability of the employed MFT approach.

3. Active magnetic regenerator cycle modeling

A magnetocaloric material's response to an external magnetic field (i.e., magnetization-demagnetization) is comparable to gas's response to compression and expansion in conventional thermodynamic refrigeration systems. However, in order to reach significant temperature differences between hot and cold heat sources, the adiabatic temperature change can be amplified using the specific active magnetic regenerator (AMR) cycle, which consists of four steps, including two adiabatic and two isofield processes (Lebouc et al., 2005).

To get insight about the implementation of $Pr_{0.6}Sr_{0.4}MnO_3$ material in an AMR device, numerical simulations of its performance are necessary. In addition to the basic concepts and equations used in the existing models of the AMRR cycle, e.g. (Allab et al., 2005; Bouchekara, 2008; Engelbrecht, 2008; Vuarnoz and Kawanami, 2012), where all the losses caused by radiation, magnetic hysteresis and eddy current are neglected, and the fluid used is incompressible with a constant physical properties, the developed one-dimensional (1D) numerical model in this study takes also into consideration the fact that the ΔT_{ad} and C_P depend on the material's temperature and the magnetic field.

3.1. Governing equations

Based on the law of energy conservation, the main equations describing the heat transfer between the solid material and the carrier fluid in a 1D model (Bouchekara and Nahas, 2012) are given by the following partial differential equations (PDEs),

$$m_f C_f \left(\frac{\partial T_f}{\partial t} + V \frac{\partial T_f}{\partial x} \right) = hS \left(T_r - T_f \right), \tag{11}$$

and

$$m_r C_r \left(B, T_r \right) \left(\frac{\partial T_r}{\partial t} + \lambda_{eff} \upsilon \frac{\partial^2 T_r}{\partial x^2} \right) = hS \left(T_f - T_r \right), \tag{12}$$

where the index f and r are related respectively to the fluid and the regenerator, C is the specific heat, T is the temperature, x is the position, t is the time, h is the heat transfer coefficient, υ is the volume of the solid and λ_{eff} is the effective thermal conductivity, it is assumed to be equal to the conductivity of the $Pr_{0.6}Sr_{0.4}MnO_3$ material, that is roughly $\lambda_{eff} \simeq \lambda_m = 1.9\, W\, m^{-1}\, K^{-1}$ (Guillou et al., 2012). This approximation is particularly appropriate when magnetocaloric materials exhibit low thermal conductivity and/or low thickness (Bouchekara, 2008). The contribution of adiabatic phases will be introduced as initial conditions for the regenerative material. In fact, at each start of the two flows, the temperature profiles in the material will be reset by,

$$T_r \left(t = 0, x \right) = T_r \left(t = \tau, x \right) \pm \Delta T_{ad} \left(B, T_r \right), \tag{13}$$

with τ is the period of fluid flow, and $\Delta T_{ad}(B, T_r)$ is the adiabatic temperature change, which depends on the material's temperature and the applied magnetic field. The sign (+) of Eq. (13) corresponds to the magnetization phase, while the sign (-) is for demagnetization.

The calculation of the exchange coefficient h requires three dimensionless numbers: (i) Reynolds number characterizing the fluid's flow, (ii) Prandle (Pr) number that depends on the fluid's physical properties, and (iii) Nusselt number. For an internal laminar flow through parallel plates, the Nusselt number is given by the following relationship (Rohsenow et al., 1998),

$$\mathrm{Nu} = h \times \frac{D_h}{\lambda_f} = 0.664 \times \mathrm{Re}^{1/2} \times \mathrm{Pr}^{1/3}, \tag{14}$$

with D_h being the hydraulic diameter of the regenerator and λ_f is the fluid thermal conductivity. The resolution of Eqs. (11) and (12) was carried out by using the finite difference method (Siddikov et al., 2005). After each cycle, the temperature profile in the fluid and the regenerator, as well as the cooling capacity are calculated, and the calculation is repeated until steady state

is reached, using a numerical program developed on MATLAB commercial software. The steady state is defined as $|T_{cold}(C_n) - T_{cold}(C_{n-1})| = |T_{hot}(C_n) - T_{hot}(C_{n-1})| = 0$ (Chiba et al., 2014), where T_{cold} and T_{hot} are the temperatures of the cold and hot sources respectively, or in another word are the temperatures of the regenerator's two ends, which correspond to x=0 and x=L with L is the length of the regenarator plates, and C is the cycle number.

3.2. Model results

The reliability of the above AMR model was validated by using extracted experimental data from the magnetic cooling prototype developed by Clean Cooling Systems SA (CCS) at the University of Applied Sciences of western Switzerland (Balli et al., 2012b; Sari and Balli, 2014). Such prototype is constituted of two parallel regenerators composed of gadolinium plates, where each regenerator is divided into two separated parts (see Fig. S1). In this paper, we mainly focus on the performance of the $Pr_{0.6}Sr_{0.4}MnO_3$ oxide when used as refrigerant in a AMR-system, which is similar to that reported in Refs. (Balli et al., 2012b; Sari and Balli, 2014). The characteristic parameters as well as the working conditions of studied $Pr_{0.6}Sr_{0.4}MnO_3$-based AMR regenerator are given in Table 2.

Fig. 4 shows the calculated temperature evolution of a regenerator composed of Gd as refrigerant compared with experimental

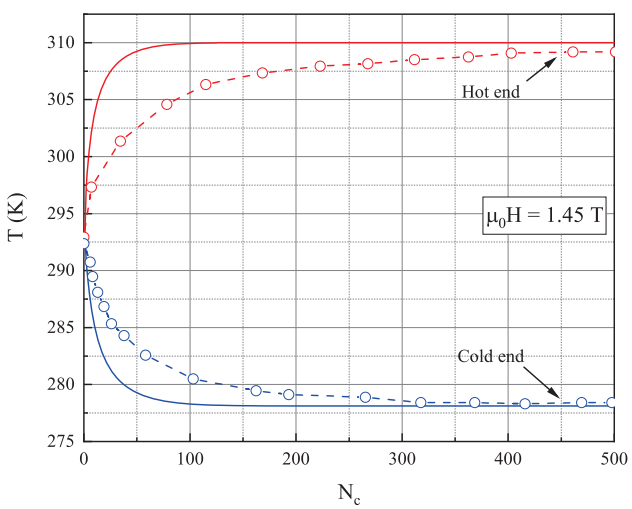

Fig. 4: Calculated (solid line) and experimental (dashed line) temperature evolution of a regenerator composed of Gd as refrigerant.

Table 2: Characteristic parameters used in the magnetic refrigerator's numerical modeling.

Heat transfer fluid	Water
Fluid flow	20 g s^{-1}
$Pr_{0.6}Sr_{0.4}MnO_3$ plates dimensions	1mm*8mm*100mm
Operation frequency	0.5 Hz
Fluid thickness	0.2 mm
Mass of MCM	800 g

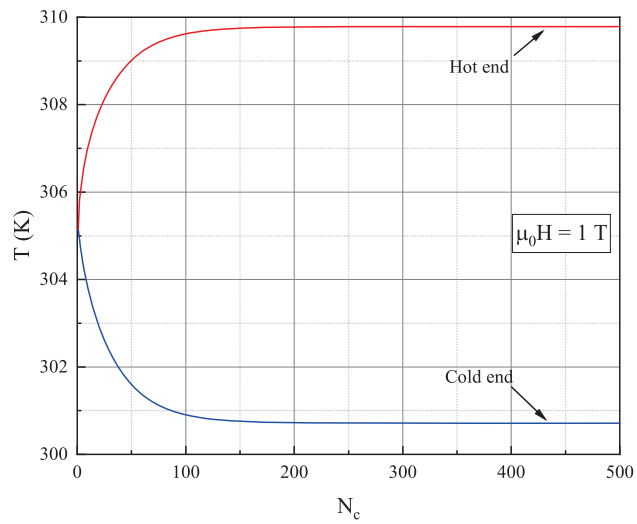

Fig. 5: Temperature evolution versus the number of cycles calculated for $Pr_{0.6}Sr_{0.4}MnO_3$ regenerator at both cold and hot ends.

measurements. Simulations on Gd indicate a good agreement with experimental data (Sari and Balli, 2014), confirming then the reliability of the used AMR model. Fig. 5 shows the temperature evolution at both sides (i.e., hot and cold ends) of the $Pr_{0.6}Sr_{0.4}MnO_3$ material as a function of the AMR cycle numbers. As can be seen, the two curves reach their steady-state after a transitory regime. The obtained maximum temperature span under a magnetic field of 1 T is about 9 K after 200 cycles. We observe that such obtained maximum temperature span is about 10 times higher than the initial ΔT_{ad}. Furthermore, in addition to the temperature span, the cooling power Q_c is one of the critical performance parameters of magnetocaloric devices, defined as the quantity of heat transferred per unit of time from the cold side to the hot side. It is given by the following relation (Chiba, 2015),

$$Q_c = \dot{m}_f C_f \left(T_c - \overline{T}_{f,c}\right), \tag{15}$$

with

$$\overline{T}_{f,c} = \frac{1}{\tau}\int_1^{\tau} T\left(x = L, t\right)\, dt. \tag{16}$$

Fig. 6(a) shows the temperature span ΔT_{span} dependence of the cooling power for the $Pr_{0.6}Sr_{0.4}MnO_3$ regenerator. High cooling powers can be generated at low-temperature spans. The maximum reached power is 17.5 W (under 1 T) for $\Delta T = 0$ K. The cooling power shows an almost linear decrease as a function of temperature span. Moreover, our simulations reveal that the implementation of $Pr_{0.6}Sr_{0.4}MnO_3$ as a refrigerant material would provide higher performance particularly under sufficiently high magnetic fields. As shown in Fig. 6(b), an almost positive linear relationship between the temperature span and the magnetic field can be observed. Furthermore, using a magnetic field source of 8 T, the $Pr_{0.6}Sr_{0.4}MnO_3$ material can generate an AMR temperature span of about 33 K. However, such a temperature difference can be obtained by using

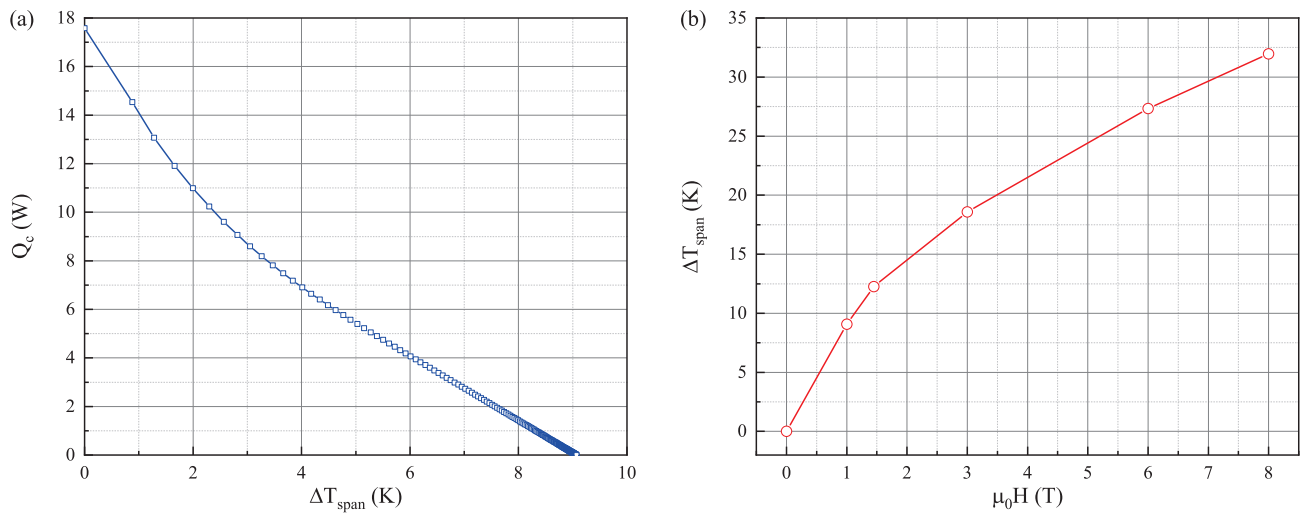

Fig. 6: (a) Cooling power versus regenerator temperature span for an applied magnetic field of 1 T. (b) Temperature span as a function of the magnetic field.

Gd metal as a refrigerant under only 1.45 T. Additionally, the temperature span ΔT_{span} evolution as a function of frequency is also evaluated (see Fig. S2).

In a magnetic refrigeration system, the expended energy mainly depends on the provided mechanical work during the magnetization-demagnetization of magnetocaloric materials and the circulation of the heat transfer fluid throughout the regenerator. In this case, the coefficient of performance (COP) is defined as the ratio of the cooling power and the input work (Kitanovski et al., 2015),

$$\mathrm{COP} = \frac{Q_c}{W_{mag} + W_{pump}}, \tag{17}$$

where W_{pump} is the fluid pumping work, and W_{mag} is the motor's magnetic work that drives the refrigerant material in and outside of the magnetic field region. Moreover, W_{pump} can be calculated using the following equation (Tishin and Spichkin, 2016),

$$W_{pump} = \frac{\dot{m} \times \Delta p}{\rho_f \times \eta_{pump}}, \tag{18}$$

where $\dot{m}$ is the mass flow rate, ρ_f is the fluid density, η_{pump} is the pump efficiency, and Δp is the pressure drop given as follows (Tishin and Spichkin, 2016),

$$\Delta p = \frac{2 f \rho_f \, (\upsilon \cdot \epsilon)^2 \, L}{D_h}, \tag{19}$$

where f is the friction factor, υ is the kinematic viscosity, ϵ is the porosity of the matrix, L is the length, and D_h is the hydraulic diameter. Moreover, W_{mag} can be expressed as follows,

$$W_{mag} = \int \vec{F} \, \vec{dl}, \tag{20}$$

where $\vec{F}$ represents the magnetic force, and $\vec{dl}$ is the displacement of the magnetocaloric material (Balli et al., 2012b).

According to Eq. (20), the determination of the magnetic work requires the calculation of involved magnetic interaction forces between the magnetocaloric regenerator and the magnetic field source. For this purpose, 3D finite-element simulations based on Flux3D software (alt) were carried out. Flux3D software uses maxwell's equations to determine the magnetic potential V_m in static condition based on the following equation,

$$div[-\mu grad(V_m) + \mu_0 M_r] = 0, \tag{21}$$

where μ_0 is the vacuum permeability, μ is the magnetic permeability, and M_r is the remanence. From this potential, all the system's magnetic characteristics can be simulated (e.g., magnetic forces, magnetic field, etc.). The simulated magnetic field source is based on the modified Halbach rotation theorem. It consists of several Nd-Fe-B permanent magnets, judiciously arranged to produce a magnetic field with the mean value of roughly 1 T as shown in Fig. 7. The magnetocaloric regenerator has the underlined characteristics in Table 2. It is magnetized and demagnetized following a linear motion. In order to estimate the involved magnetic interaction forces during the magnetization/demagnetization phases, it is necessary to provide the exact orientation and geometry of the $Pr_{0.6}Sr_{0.4}MnO_3$ plates as well as their relative magnetic permeability. The latter is given by (Balli et al., 2011),

$$\mu_r = 1 + \chi = 1 + \frac{M}{H}, \tag{22}$$

where M represents the magnetization, H is the external applied field and χ is the magnetic susceptibility, which is deduced from the magnetization isotherm curves reported in Fig. 1(a). For $Pr_{0.6}Sr_{0.4}MnO_3$ compound, the relative permeability around its T_c = 305 K is found to be approximately 1.2.

The experienced forces by the $Pr_{0.6}Sr_{0.4}MnO_3$ regenerator during the magnetization-demagnetization cycle are shown in Fig. 7(b). The associated magnetic work is deduced from Eq.

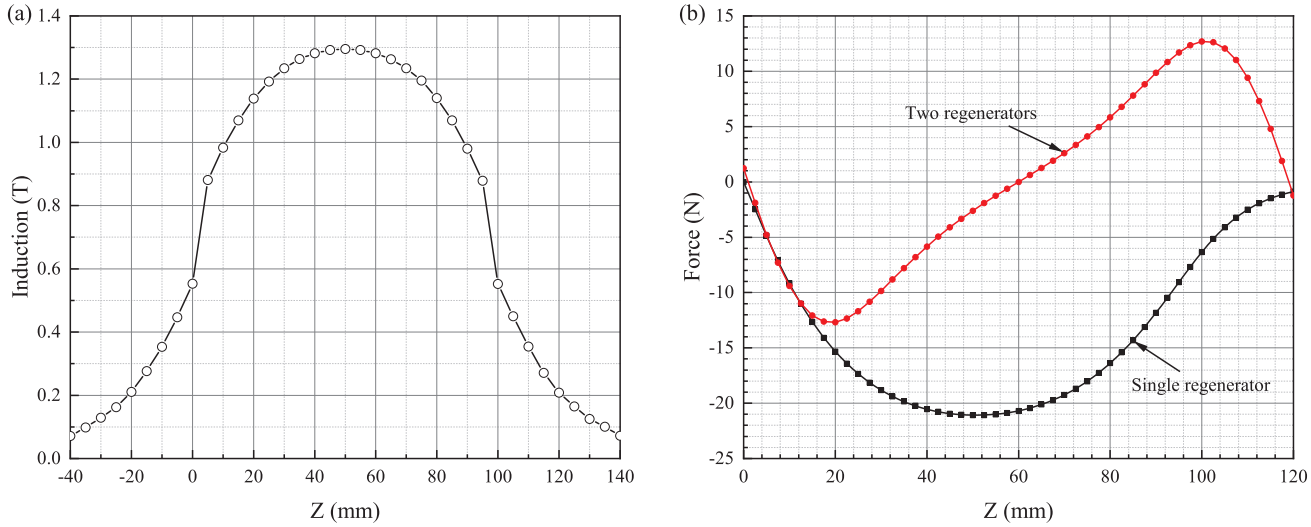

Fig. 7: (a) Magnetic induction distribution along the magnetic source' axis. (b) Magnetic forces as a function of active material displacement in the cases of single and balanced regenerators.

(20) while the pump work is calculated with the help of Eq. (19), which leads to a maximum COP of 0.5 under 1 T. However, in order to reduce the magnetic work, the regenerator is divided into two parts separated by a distance of 20 mm. In this case, when the first part of the regenerator is demagnetized, the second part is automatically magnetized (see Fig. S1), which allows us to balance the magnetic forces, as can be clearly seen in Fig. 7(b). Consequently, the magnetic work is reduced by 80 %, increasing thus markedly the maximum COP of $Pr_{0.6}Sr_{0.4}MnO_3$ regenerator that reaches about 1. From a practical point of view, this value is comparable with the maximum COP that can be reached by a conventional refrigerator (Sari and Balli, 2014). However, larger COP can be obtained by inducing large thermal effects in the $Pr_{0.6}Sr_{0.4}MnO_3$ regenerator, which would be achieved by subjecting the latter to high magnetic fields and/or strain effects (Bouhani et al., 2020). From obtained results, it is clearly observed that the coefficient of performance for $Pr_{0.6}Sr_{0.4}MnO_3$ is lower than that of Gd (Chiba et al., 2014), under similar working conditions. This is mainly due to the relatively moderate magnetocaloric effect exhibited by the $Pr_{0.6}Sr_{0.4}MnO_3$ oxide which is about 3 times lower than that of Gd. However, even though the $Pr_{0.6}Sr_{0.4}MnO_3$ oxides exbibit low magnetocaloric performance when compared to the benchmark Gd material, their magnetic and magnetocaloric properties can be improved and modulated through both chemical and mechanical effects. On the other hand, this family of materials shows additional practical advantages such as high chemical stability, lower thermal and field hysteresis, lower cost of constituent elements, and high electrical resistance that prevents eddy currents.

4. Theoretical limit assessment

In order to explore the hidden thermodynamic performances of $Pr_{0.6}Sr_{0.4}MnO_3$, we theoretically raised the external magnetic field until the complete order of its magnetic moments was achieved. Fig. 8(a) represents the adiabatic temperature change as function of temperature. The inset indicates the magnetic entropy change calculated by MFT for both standard conditions and near the theoretical limit case. At room temperature, the limit values of adiabatic temperature and isothermal entropy changes were found to be as high as 29 K and 12.5 J mol^{-1} K^{-1} (57 J kg^{-1} K^{-1}), respectively. These values are 30 times larger than those calculated in the practical magnetic field of 1.5 T. However, unrealistic magnetic fields of about 1500 T are needed to attain such high MCE values. Using the above AMR-numerical model, the performance of $Pr_{0.6}Sr_{0.4}MnO_3$ are also investigated over the theoretical limit region of its MCE. For this purpose, the gaseous helium is used as carrier fluid which enables us to avoid the drawbacks associated with the water freezing. First, we have plotted the helium's physical properties as a function of temperature (Hel), then we have fitted the results to obtain the characteristic equations. The latters were integrated in the AMR model, to simulate the device operation using helium as a heat transfer fluid. Fig. 8(b) represents the temperature evolution at both cold and hot sources as a function of cycles number. In this way, our calculation reveals that after just 25 min, a cold source temperature under −22 °C and a span of about 112 °C can be reached. Lower temperatures and greater spans would be obtained if the steady-state is achieved. On the other hand, the temperature span present a similar feature to the one reported in Ref. (Zhang et al., 2010) for a reciprocating magnetic cooling machine that uses Gd as refrigerant and helium as a heat transfer fluid.

Of course, the application of high magnetic fields to reach the MCE theoretical limit in $Pr_{0.6}Sr_{0.4}MnO_3$ is out of question due to the required unrealistic values (1500 T). However, outstanding thermal effects could be generated by taking advantage of the coupling between different degrees of freedom in this family

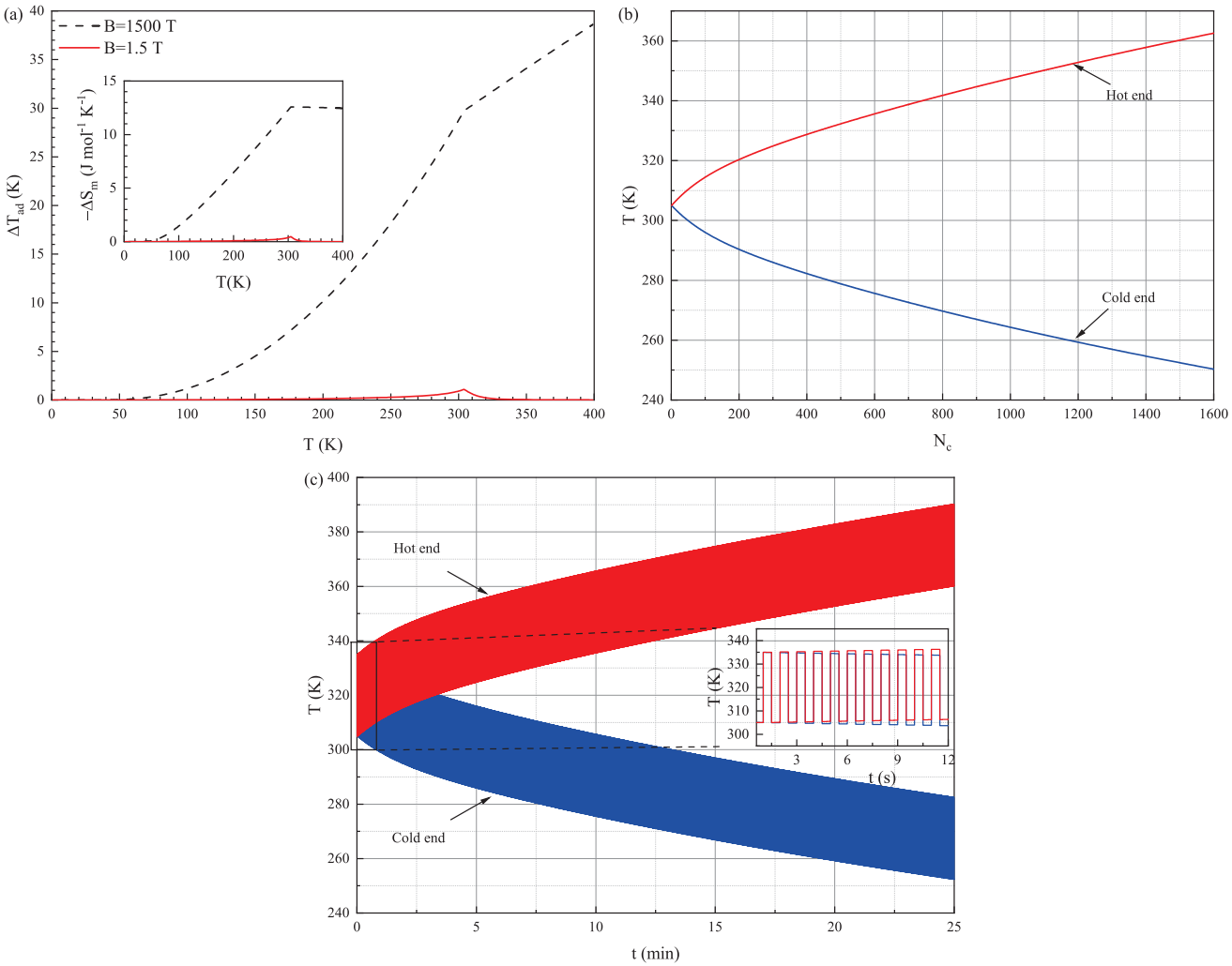

Fig. 8: (a) Calculated adiabatic temperature changes as a function of temperature for $Pr_{0.6}Sr_{0.4}MnO_3$ under 1.5 T and 1500 T. The inset displays the associated magnetic entropy variation. (b) Temperature spans calculated in the case where the helium is chosen as heat transfer fluid. (c) Time evolution of the solid temperature at both cold and hot ends. The inset displays the beginning of the cycles.

of materials, involving structural, electronic, orbital, and magnetic ordering parameters. For example, the simultaneous application of several excitations such as magnetic field, electrical field and strain effects would lead to unusual MCEs. In a recently reported work, Bouhani et *al.* (Bouhani et al., 2020) were able to induce in $PrVO_3$ thin films a magnetic entropy change that approaches the theoretical limit when subjecting them to strain effects. Consequently, this would open the way for boosting the MCE in the family of strongly correlated materials such as $RMnO_3$ manganites.

5. Conclusions and outlook

In this work, the magnetic and magnetocaloric properties of $Pr_{0.6}Sr_{0.4}MnO_3$ oxide as well as their performance in a AMR-system were studied to figure out its real potential in magnetic cooling. The needed magnetocaloric parameters such as specific heat, magnetization, adiabatic temperature change, and entropy change were calculated in the framework of Mean Field Theory. The letter seems to be a good approach for predicting the magnetic and magnetocaloric properties of $Pr_{0.6}Sr_{0.4}MnO_3$ oxide, unveiling thus the localized feature of the magnetism in this compound. On the other hand, we have discovered that the use of Neumann & Kopp's law gives a good predictions of C_L near to the ambient temperature. Besides, AMR simulations reveal that a maximum temperature span of 9 K, a maximum cooling power of about 17.5 W, and a maximum COP of 0.5 can be achieved under the practical magnetic field of 1 T. However, such performance can be markedly amplified by balancing magnetic forces in the regenerator. In fact, when the latter is divided into two separated parts, the COP becomes twice larger in a similar magnetic field. On the other hand, it was observed that the temperature span increases linearly with magnetic field to reach a value of 33 K under 8 T. But, such a temperature difference can be achieved by using gadolinium metal under only about 1.45 T, which is mainly due to the large adiabatic temper-

ature change shown by this rare-earth element. Furthermore, the performance of $Pr_{0.6}Sr_{0.4}MnO_3$ oxide close to the theoretical limit of its MCE were also carried out. Particularly, it was found that in this case, cold temperatures under -22 °C can be reached by using only the gaseous helium as carrier fluid. Unfortunately, unrealistic magnetic fields of roughly 1500 T calculated by using MFT are required to attain the MCE theoretical limit in $Pr_{0.6}Sr_{0.4}MnO_3$. The achieved results will open the way to the search for other practical alternative stimulus such as strain effects to attain such limit, as demonstrated in our recently reported work.

Acknowledgments

O. Chdil and M. Balli acknowledge funding by the International University of Rabat. O. Chdil greatly appreciate the important discussion with Professor Y. Chiba from the Faculty of Science and Technology, University of Medea, Algeria.

References

, . Altair flux overview. https://www.altair.com/flux/. Accessed: 2021-04-22.

, . Thermal conductivity of gases chart. https://www.engineersedge.com/heat_transfer/thermal-conductivity-gases.htm. Accessed: 2021-04-22.

Alahmer, A., Al-Amayreh, M., Mostafa, A.O., Al-Dabbas, M., Rezk, H., 2021. Magnetic refrigeration design technologies: State of the art and general perspectives. Energies 14, 4662.

Allab, F., Kedous-Lebouc, A., Fournier, J.M., Yonnet, J.P., 2005. Numerical modeling for active magnetic regenerative refrigeration. IEEE transactions on magnetics 41, 3757–3759.

Aprea, C., Greco, A., Maiorino, A., Masselli, C., 2015. A comparison between rare earth and transition metals working as magnetic materials in an amr refrigerator in the room temperature range. Applied Thermal Engineering 91, 767–777.

Bahl, C.R., Velázquez, D., Nielsen, K.K., Engelbrecht, K., Andersen, K.B., Bulatova, R., Pryds, N., 2012. High performance magnetocaloric perovskites for magnetic refrigeration. Applied Physics Letters 100, 121905.

Balli, M., Jandl, S., Fournier, P., Kedous-Lebouc, A., 2017. Advanced materials for magnetic cooling: Fundamentals and practical aspects. Applied Physics Reviews 4, 021305.

Balli, M., Jandl, S., Fournier, P., Vermette, J., Dimitrov, D., 2018. Unusual rotating magnetocaloric effect in the hexagonal $ErMnO_3$ single crystal. Physical Review B 98, 184414.

Balli, M., Mahmed, C., Bonhote, P., Sari, O., 2011. On the magnetic forces in magnetic cooling machines: Numerical calculations and experimental investigations. IEEE transactions on magnetics 47, 3383–3386.

Balli, M., Mahmed, C., Duc, D., Nikkola, P., Sari, O., Hadorn, J.C., Rahali, F., 2012a. Le renouveau de la réfrigération magnétique. Revue Générale du Froid 102, 45–54.

Balli, M., Sari, O., Mahmed, C., Besson, C., Bonhote, P., Duc, D., Forchelet, J., 2012b. A pre-industrial magnetic cooling system for room temperature application. Applied Energy 98, 556–561.

Barclay, J., 1982. Theory of an active magnetic regenerative refrigerator. Technical Report. Los Alamos National Lab., NM (USA).

Barik, S., Krishnamoorthi, C., Mahendiran, R., 2011. Effect of fe substitution on magnetocaloric effect in La0.7Sr0.3Mn1 − xFexO$_3$ (0.05≤ x≤ 0.20). Journal of Magnetism and Magnetic Materials 323, 1015–1021.

Barik, S., Mahendiran, R., 2010. Effect of bi doping on magnetic and magnetocaloric properties of $La_{0.7-x}Bi x Sr_{0.3}MnO_3$ (0≤ x≤ 0.4). Journal of Applied Physics 107, 093906.

Barman, A., Kar-Narayan, S., Mukherjee, D., 2019. Caloric effects in perovskite oxides. Advanced Materials Interfaces 6, 1900291.

Bingham, N., Phan, M., Srikanth, H., Torija, M., Leighton, C., 2009. Magnetocaloric effect and refrigerant capacity in charge-ordered manganites. Journal of Applied Physics 106, 023909.

Bouchekara, H., Nahas, M., 2012. Magnetic refrigeration technology at room temperature, in: Trends in Electromagnetism-From Fundamentals to Applications. InTech.

Bouchekara, H.R.E.H., 2008. Recherche sur les systèmes de réfrigération magnétique. Modélisation numérique, conception et optimisation. Ph.D. thesis.

Bouhani, H., Endichi, A., Kumar, D., Copie, O., Zaari, H., David, A., Fouchet, A., Prellier, W., Mounkachi, O., Balli, M., et al., 2020. Engineering the magnetocaloric properties of $PrVO_3$ epitaxial oxide thin films by strain effects. Applied Physics Letters 117, 072402.

Brown, G., 1976. Magnetic heat pumping near room temperature. Journal of Applied Physics 47, 3673–3680.

Brück, E., 2005. Developments in magnetocaloric refrigeration. Journal of Physics D: Applied Physics 38, R381.

Chiba, Y., 2015. Contribution à l'étude d'un réfrigérateur à régénération magnétique active opérant près de la température ambiante: considérations thermo fluides. Ph.D. thesis. Ecole Nationale Polytechnique d'Alger; Fachhochschule Westschweiz.

Chiba, Y., Smaïli, A., Mahmed, C., Balli, M., Sari, O., 2014. Thermal investigations of an experimental active magnetic regenerative refrigerator operating near room temperature. International journal of refrigeration 37, 36–42.

Chmaissem, O., Dabrowski, B., Kolesnik, S., Mais, J., Jorgensen, J., Short, S., 2003. Structural and magnetic phase diagrams of $La_{1-x}Sr_xMnO_3$ and $Pr_{1-y}Sr_yMnO_3$. Physical Review B 67, 094431.

Daivajna, M.D., Kumar, N., Awana, V., Gahtori, B., Christopher, J.B., Manjunath, S., Syu, K., Kuo, Y., Rao, A., 2014. Electrical, magnetic and thermal properties of $Pr_{0.6-x}Bi_xSr_{0.4}MnO_3$ manganites. Journal of alloys and compounds 588, 406–412.

Daivajna, M.D., Rao, A., 2016. Magnetocaloric effect in pristine and Bi-doped $Pr_{0.6}Sr_{0.4}MnO_3$ manganite. Solid State Communications 245, 65–69.

Dall'Olio, S., Masche, M., Liang, J., Insinga, A., Eriksen, D., Bjørk, R., Nielsen, K., Barcza, A., Vieyra, H., Beek, N.v., et al., 2021. Novel design of a high efficiency multi-bed active magnetic regenerator heat pump. International Journal of Refrigeration .

Dan'Kov, S.Y., Tishin, A., Pecharsky, V., Gschneidner, K., et al., 1998. Magnetic phase transitions and the magnetothermal properties of gadolinium. Physical Review B 57, 3478.

De Oliveira, N., Von Ranke, P., 2010. Theoretical aspects of the magnetocaloric effect. Physics Reports 489, 89–159.

Dupont, J.L., Domanski, P., Lebrun, P., Ziegler, F., 2019. « Le froid est essentiel pour l'humanité et doit devenir une priorité des décideurs politiques.». Note d'Information de l'IIF 38.

Engelbrecht, K., 2008. A numerical model of an active magnetic regenerator with experimental validation. Ph. D. Thesis, University of Wisconsin-Madison .

Engelbrecht, K., Bahl, C.R.H., Nielsen, K.K., 2011. Experimental results for a magnetic refrigerator using three different types of magnetocaloric material regenerators. International Journal of refrigeration 34, 1132–1140.

Eustache, J., Plait, A., Dubas, F., Glises, R., 2021. Review of multi-physics modeling on the active magnetic regenerative refrigeration. Mathematical and Computational Applications 26, 47.

Franco, V., Blázquez, J., Ingale, B., Conde, A., 2012. The magnetocaloric effect and magnetic refrigeration near room temperature: materials and models. Annual Review of Materials Research 42.

Franco, V., Blázquez, J., Ipus, J., Law, J., Moreno-Ramírez, L., Conde, A., 2018. Magnetocaloric effect: From materials research to refrigeration devices. Progress in Materials Science 93, 112–232.

Ghodhbane, S., Dhahri, A., Dhahri, N., Hlil, E.K., Dhahri, J., 2013. Structural, magnetic and magnetocaloric properties of $La_{0.8}Ba_{0.2}Mn_{1-x}Fe_xO_3$ compounds with 0≤ x≤ 0.1. Journal of alloys and compounds 550, 358–364.

Giri, S., MacManus-Driscoll, J., Li, W., Wu, R., Nath, T., Maity, T., 2019. Strain induced extrinsic magnetocaloric effects in $La_{0.67}Sr_{0.33}MnO_3$ thin films, controlled by magnetic field. Journal of Physics D: Applied Physics 52, 165302.

Gottschall, T., Kuz'Min, M., Skokov, K., Skourski, Y., Fries, M., Gutfleisch, O., Zavareh, M.G., Schlagel, D.L., Mudryk, Y., Pecharsky, V., et al., 2019a. Magnetocaloric effect of gadolinium in high magnetic fields. Physical Review B 99, 134429.

Gottschall, T., Skokov, K.P., Fries, M., Taubel, A., Radulov, I., Scheibel, F., Benke, D., Riegg, S., Gutfleisch, O., 2019b. Making a cool choice: the materials library of magnetic refrigeration. Advanced Energy Materials 9,

1901322.
Greco, A., Aprea, C., Maiorino, A., Masselli, C., 2019. A review of the state of the art of solid-state caloric cooling processes at room-temperature before 2019. International Journal of Refrigeration 106, 66–88.
Gschneidner Jr, K.A., Pecharsky, V., Tsokol, A., 2005. Recent developments in magnetocaloric materials. Reports on progress in physics 68, 1479.
Guillou, F., Legait, U., Kedous-Lebouc, A., Hardy, V., 2012. Development of a new magnetocaloric material used in a magnetic refrigeration device, in: EPJ Web of Conferences, EDP Sciences. p. 00021.
Huang, B., Lai, J., Zeng, D., Zheng, Z., Harrison, B., Oort, A., van Dijk, N., Brück, E., 2019. Development of an experimental rotary magnetic refrigerator prototype. International Journal of Refrigeration 104, 42–50.
Ismail, M., Yebiyo, M., Chaer, I., 2021. A review of recent advances in emerging alternative heating and cooling technologies. Energies 14, 502.
Kamran, M.S., Ahmad, H.O., Wang, H.S., 2020. Review on the developments of active magnetic regenerator refrigerators–evaluated by performance. Renewable and Sustainable Energy Reviews 133, 110247.
Kitanovski, A., 2020. Energy applications of magnetocaloric materials. Advanced Energy Materials 10, 1903741.
Kitanovski, A., Plaznik, U., Tomc, U., Poredoš, A., 2015. Present and future caloric refrigeration and heat-pump technologies. International Journal of Refrigeration 57, 288–298.
Kitanovski, A., Plaznik, U., Tušek, J., Poredoš, A., 2014. New thermodynamic cycles for magnetic refrigeration. International journal of refrigeration 37, 28–35.
Kopp, H., Graham, T., 1865. III. investigations of the specific heat of solid bodies. Philosophical Transactions of the Royal Society of London 155, 71–202.
Du Trémolet de Lacheisserie, É., Gignoux, D., Schlenker, M., 2005. Magnetism: Fundamentals.
Lebouc, A., Allab, F., Fournier, J.M., Yonnet, J.P., 2005. Réfrigération magnétique. Techniques de l'Ingénieur .
Lees, M., Petrenko, O., Balakrishnan, G., Paul, D.M., 1999. Specific heat of $Pr_{0.6}(Ca_{1-x}Sr_x)_{0.4}MnO_3$ ($0 \leqslant x \leqslant 1$). Physical Review B 59, 1298.
Legait, U., Guillou, F., Kedous-Lebouc, A., Hardy, V., Almanza, M., 2014. An experimental comparison of four magnetocaloric regenerators using three different materials. International Journal of Refrigeration 37, 147–155.
Maheswar Repaka, D., Tripathi, T., Aparnadevi, M., Mahendiran, R., 2012. Magnetocaloric effect and magnetothermopower in the room temperature ferromagnet $Pr_{0.6}Sr_{0.4}MnO_3$. Journal of Applied Physics 112, 123915.
Martin, C., Maignan, A., Hervieu, M., Raveau, B., 1999. Magnetic phase diagrams of $L_{1-x}A_xMnO_3$ manganites (L= Pr, Sm; A= Ca, Sr). Physical Review B 60, 12191.
Matte, D., de Lafontaine, M., Ouellet, A., Balli, M., Fournier, P., 2018. Tailoring the magnetocaloric effect in La_2NiMnO_6 thin films. Physical Review Applied 9, 054042.
Molina, M.J., Rowland, F.S., 1974. Stratospheric sink for chlorofluoromethanes: chlorine atom-catalysed destruction of ozone. Nature 249, 810–812.
Moya, X., Hueso, L., Maccherozzi, F., Tovstolytkin, A., Podyalovskii, D., Ducati, C., Phillips, L., Ghidini, M., Hovorka, O., Berger, A., et al., 2013. Giant and reversible extrinsic magnetocaloric effects in $La_{0.7}Ca_{0.3}MnO_3$ films due to strain. Nature materials 12, 52–58.
Moya, X., Kar-Narayan, S., Mathur, N.D., 2014. Caloric materials near ferroic phase transitions. Nature materials 13, 439–450.
Nielsen, K.K., Tusek, J., Engelbrecht, K., Schopfer, S., Kitanovski, A., Bahl, C.R.H., Smith, A., Pryds, N., Poredos, A., 2011. Review on numerical modeling of active magnetic regenerators for room temperature applications. International Journal of Refrigeration 34, 603–616.
Petersen, T.F., Engelbrecht, K., Bahl, C.R., Elmegaard, B., Pryds, N., Smith, A., 2008. Comparison between a 1D and a 2D numerical model of an active magnetic regenerative refrigerator. Journal of Physics D: Applied Physics 41, 105002.
Phan, M.H., Peng, H.X., Yu, S.C., 2005a. Large magnetocaloric effect in single crystal $Pr_{0.63}Sr_{0.37}MnO_3$. Journal of applied physics 97, 10M306.
Phan, M.H., Yu, S.C., 2007. Review of the magnetocaloric effect in manganite materials. Journal of Magnetism and Magnetic Materials 308, 325–340.
Phan, M.H., Yu, S.C., Hur, N.H., 2005b. Excellent magnetocaloric properties of $La_{0.7}Ca_{0.3-x}Sr_xMnO_3$ ($0.05 \leq x \leq 0.25$) single crystals. Applied Physics Letters 86, 072504.
Protocol, M., 1987. Montreal protocol on substances that deplete the ozone layer. Washington, DC: US Government Printing Office 26, 128–136.
Rocco, D., Coelho, A., Gama, S., Santos, M.d.C., 2013. Dependence of the magnetocaloric effect on the A-site ionic radius in isoelectronic manganites. Journal of Applied Physics 113, 113907.
Rohsenow, W.M., Hartnett, J.P., Cho, Y.I., et al., 1998. Handbook of heat transfer. volume 3. McGraw-Hill New York.
Sakka, A., M'nassri, R., Chniba-Boudjada, N., Ommezzine, M., Cheikhrouhou, A., 2016. Effect of trivalent rare earth doping on magnetic and magnetocaloric properties of $Pr_{0.5}(Ce, Eu, Y)_{0.1}Sr_{0.4}MnO_3$ manganites. Applied Physics A 122, 603.
Sari, O., Balli, M., 2014. From conventional to magnetic refrigerator technology. International journal of refrigeration 37, 8–15.
Seinfeld, J.H., Pandis, S.N., 2016. Atmospheric chemistry and physics: from air pollution to climate change. John Wiley & Sons.
Siddikov, B., Wade, B., Schultz, D., 2005. Numerical simulation of the active magnetic regenerator. Computers & Mathematics with Applications 49, 1525–1538.
Silva, D.J., Ventura, J., Araújo, J.P., 2021. Caloric devices: A review on numerical modeling and optimization strategies. International Journal of Energy Research .
Smith, A., Bahl, C.R., Bjørk, R., Engelbrecht, K., Nielsen, K.K., Pryds, N., 2012. Materials challenges for high performance magnetocaloric refrigeration devices. Advanced Energy Materials 2, 1288–1318.
Tagliafico, G., Scarpa, F., Canepa, F., 2010. A dynamic 1-d model for a reciprocating active magnetic regenerator; influence of the main working parameters. International journal of refrigeration 33, 286–293.
Tishin, A.M., Spichkin, Y.I., 2016. The magnetocaloric effect and its applications. CRC Press.
Trevizoli, P.V., Nakashima, A.T., Peixer, G.F., Barbosa Jr, J.R., 2017. Performance assessment of different porous matrix geometries for active magnetic regenerators. Applied Energy 187, 847–861.
Tušek, J., Kitanovski, A., 2015. Magnetocaloric energy conversion: From theory to applications.
Velders, G.J., Fahey, D.W., Daniel, J.S., McFarland, M., Andersen, S.O., 2009. The large contribution of projected HFC emissions to future climate forcing. Proceedings of the National Academy of Sciences 106, 10949–10954.
Vuarnoz, D., Kawanami, T., 2012. Numerical analysis of a reciprocating active magnetic regenerator made of gadolinium wires. Applied Thermal Engineering 37, 388–395.
Waske, A., Gruner, M.E., Gottschall, T., Gutfleisch, O., 2018. Magnetocaloric materials for refrigeration near room temperature. MRS Bulletin 43, 269–273.
Yu, B., Liu, M., Egolf, P.W., Kitanovski, A., 2010. A review of magnetic refrigerator and heat pump prototypes built before the year 2010. International Journal of refrigeration 33, 1029–1060.
Zarkevich, N.A., Zverev, V.I., 2020. Viable materials with a giant magnetocaloric effect. Crystals 10, 815.
Zhang, H., Shen, J., Gong, M.Q., Wu, J.F., 2010. Cooling performance of a room-temperature magnetic refrigerator prototype. Journal of Applied Physics 107, 09A937.
Zhang, Y., Wu, J., He, J., Wang, K., Yu, G., 2021. Solutions to obstacles in the commercialization of room-temperature magnetic refrigeration. Renewable and Sustainable Energy Reviews 143, 110933.

View publication stats